J Mater Sci (2011) 46:2212–2220
DOI 10.1007/s10853-010-5059-2

Study on growth of hollow nanoparticles of alumina

Naveen V. Kulkarni · Soumen Karmakar · Srinanadan N. Asthana · Ashok B. Nawale · Arif Sheikh · Shashikant P. Patole · J. B. Yoo · Vikas L. Mathe · Ashok K. Das · Sudha V. Bhoraskar

Received: 23 April 2010 / Accepted: 9 November 2010 / Published online: 30 November 2010

Abstract This article addresses the growth of hollow nanocrystalline particles of γ-alumina by the post-oxidation of nano-aluminium particles in air. The nanoparticles of aluminium were synthesized in a DC-transferred arc thermal plasma reactor. The as-synthesized nano-aluminium particles were oxidized, in air, at different temperatures. The as-synthesized parent nano aluminium and their daughter nanoparticles of aluminium oxide were thoroughly characterized with the help of X-ray diffraction analysis, high resolution transmission electron microscopy and thermogravimetric analysis. Two-step oxidation behaviours, unique in nanoparticles, are found to be the main driving force behind the formation of hollow spherical structures. The entire phenomenon is compared with the oxidation behaviour of coarse grain aluminium. The content of γ-alumina, identified by X-ray diffraction, relative to that of unreacted aluminium, has increased almost exponentially with the oxidation temperature in the case of nano aluminium. Similar behaviour is not observed in the case of coarse grain aluminium. The crystalline features of alumina, forming the walls of the hollow sphere, were confirmed by high resolution transmission electron microscopy.

N. V. Kulkarni · S. Karmakar · A. B. Nawale · A. Sheikh · V. L. Mathe (✉) · S. V. Bhoraskar
Department of Physics, University of Pune, Pune 411007, India
e-mail: vlmathe@physics.unipune.ac.in

S. N. Asthana
High Energy Materials Research Laboratory, Pune 411021, India

S. P. Patole · J. B. Yoo
SKKU Advanced Institute of Nanotechnology, Sungkyunkwan University, Suwon 440-746, Korea

A. K. Das
Laser and Plasma Technology Division, Bhabha Atomic Research Center, Mumbai 85, India

Introduction

'Nanophase ceramics' is a major thrust area in the current scientific and industrial community in view of the performance behaviour related to particle size characteristics [1–6]. Ultrafine alumina powder has considerable potential for a wide range of applications, including high-strength materials, electronic ceramics and catalytic support [7–9]. This interesting ceramic material exists in eight different polymorphs, of which seven (γ, δ, κ, ρ, η, θ and χ) are metastable transition phases which are unstable at room temperature and one (α) thermally stable phase [10]. Amongst the transition phases, γ-alumina is often used as support catalyst in the industry. The support material should have a large specific surface area, and in some cases, must withstand high temperature. Hirayama [11] found that the spherical γ-alumina particles can withstand temperatures higher than that for any of the commercial aluminas. Moreover, it has been reported that due to the size-dependent phase stability, the transition phases are preferred by the small particles with diameters of a few nanometres [12]. Consequently nanocrystalline γ-alumina has significant application potential.

Apart from their direct applications, nanoparticles of Al_2O_3 have been characterized as dispersoids [13], and are often synthetically added to enhance the yield strength and creep-resistance, of the host matrix. Since the most important application of Al_2O_3 arises from its catalytic properties, hollow nanoparticles of γ-alumina are expected to provide improved catalytic reactions with added low density properties.

From this point of view we report a simple process to grow spherical hollow nanoparticles of alumina with a much higher value of specific surface area. The literature shows that hollow particles have always been promising, and various attempts have been made to grow them by different routes. Role of oxygen diffusion in nanoparticles has been found to be dominant phenomenon leading to the oxidation in metals [14]. Recently morphology of hollow metal particles like Zn, Al, Cu, Ni and Fe have been studied using Transmission Electron Microscopy (TEM) [15], wherein, faster outward diffusion of metal ions through the oxide layer has been set responsible to the formation of hollow particles. Eun et al. [16] followed the capillary flow method to grow micrometre-sized hollow spheres of TiO_2 whereas Lee and Lee [17] synthesized hollow nanoparticles of TiO_2, Fe_2O_3 and Al_2O_3 via gas phase synthesis using acetylacetonate precursor. Transmittance of TiO_2 hollow nanoparticles was measured to determine their suitability for optical applications. Li et al. [18] have shown that hollow spheres of WO_3, synthesized by solution phase using templates, turned out to be highly sensitive gas sensors. The fabrication of the micro core structure of SiO_2, Al_2O_3 and TiO_2 from hydrophobic solvents has been reported by Guo et al. [19]. Kou et al. [20] synthesized hollow microsphere of Al_2O_3 by calcinations of $Al/AlOOH{\cdot}nH_2O$ core–shell particles using the wet chemical method. On the other hand, hollow micro spheres of SiO_2, using pollen grain as a bio-template, have been synthesized by Cao and Li [21] for improving the physical adsorption properties. Hollow particles of yttria were grown by Pravdic and Gani [22] using dc plasma jet. These routes are complicated and leave behind chemical by-products; whereas, this article reports a two-step synthesis procedure of hollow nanoparticles of γ-alumina by the post-oxidation of nano Al, synthesized by thermal plasma-assisted gas phase reaction. The importance of this method lies in the absence of any hazardous chemical as well as any chemical by-product. The procedure is fully secure physically, whereas the production rate is controllable in a large scale.

X-Ray Diffraction (XRD) analysis of the oxidized particles helped in observing the sequential conversion of aluminium into its oxide. The morphology of the resulting hollow particles was ascertained by TEM. High resolution TEM (HRTEM) lattice imaging of the shell walls was seen to correlate closely with the lattice spacing in the gamma phase of alumina. The oxidation behaviour of nano-aluminium particles leading to the hollow γ-alumina was further investigated with thermogravimetric studies. The discussion of the two-step oxidation process leading into the hollow γ-alumina is presented here. Subsequently the surface area for the hollow γ-alumina was studied by the single point BET method.

Experiments

The synthesis methodology of hollow nanocrystalline γ-alumina consisted of two major steps: (a) synthesis of nano aluminium by Direct Current Transferred Arc Thermal Plasma Reactor (DCTATPR) and (b) the post-oxidation of the synthesized nano aluminium.

The precursor for nano aluminium was 99% pure aluminium. It was made to evaporate by a transferred arc thermal plasma jet inside a reactor which is discussed in our earlier communication [23]. The operating parameters chosen for the synthesis of nano aluminium are shown in Table 1.

The as-synthesized nanocrystalline aluminium particles were collected from the water cooled hemispherical dome after bringing the reactor to the ambient temperature. For passivating the as-synthesized nanoparticles of Al with a thin oxide layer the atmospheric air was purged into the reactor and maintained at a pressure of 1 Torr for 5 min before opening the chamber.

The as-synthesized sample of nano aluminium was thoroughly crushed and heated to a desired temperature in the ambient air. The temperature was achieved by heating with a temperature ramp of 10 °C/min. After reaching the desired temperature, the corresponding sample was held at that temperature for about 10 min. After cooling down the furnace to room temperature, the oxidized nano-aluminium powder was collected and characterized. To study the oxidation behaviour of nano aluminium, five different batches of nano aluminium were heated in air at ambient pressure at five different temperatures, namely, 200, 400, 600, 800 and 1000 °C as explained above. A similar experiment was also carried out with commercially available coarse-grain aluminium having average particle size of 20 μm powder (Kemphasol, Mumbai India) so as to

Table 1 Operating parameters of the reactor during the synthesis of nano Al

No.	Particulars	
1.	Plasma forming gas	Nitrogen
2.	Flow rate of plasma forming gas (L/m)[a]	5
3.	Arc current (A)	200
4.	Arc length (mm)	50
5.	Arc voltage (V)	40
6.	Temperature of collector dome (°C)	30
7.	Base pressure in reactor (Torr)[b]	0.001
8.	Operating pressure in reactor (Torr)[b]	250
9.	Yield of production	50 g/h

[a] 1 L/m (Litre/min) = 17×10^{-6} m^3s^{-1}

[b] 1 Torr = 133 Nm^{-2}

compare the phenomenon of oxidation in nano aluminium with that of the micro-aluminium particles.

The parent nano aluminium, the micro-aluminium powder and the corresponding oxides were characterized by XRD using the 'Brucker D-8 X-ray diffractometer' and TEM (JEOL 300 kV). For carrying out TEM analysis 2 mg of the sample was thoroughly dispersed in 5 mL of acetonitrile solution mild sonication for about 30 min. A tiny drop of the solution was then placed on a carbon coated copper grid and completely dried, before analysis.

Results and discussion

Phase and structural investigation by X-ray diffraction analysis

Nanoparticles of aluminium formed precursors for the synthesis of hollow γ-alumina and thus it was necessary to ascertain the crystalline structure of the as-synthesized and subsequently oxidized particles using XRD analysis.

The XRD pattern of as-synthesized powder is shown in Fig. 1a. The diffraction pattern closely resembles the standard JCPDS data of c-Al [24] shown by the dotted line pattern at the bottom of the diagram. The standard line intensity pattern (obtained from JCPDS data) for γ-alumina [24] (solid line) is also shown. A careful observation showed that the oxide species in the product particles resembled only the γ-alumina, and hence the standard lines of only this crystalline phase have been compared. The XRD pattern of nanoparticles oxidized at different, steady temperatures, 200–1000 °C in steps of 200 °C are presented as b–f in Fig. 1a. After comparing the line positions with those of standard data we infer that the line intensities corresponding to γ-Al_2O_3 increase with increasing oxidation temperature. Moreover, the lines are much broader for samples oxidized beyond 600 °C, which indicates that the observed species have been reduced dimensions.

The major lines corresponding to Al at $2\theta = 38.4°$, 44.7° and 65.1° are seen to fall in intensity upon oxidation at 800 °C, whereas, they have disappeared at 1000 °C. The lines corresponding to γ-Al_2O_3 at $2\theta = 31.9°$, 37.6°, 46°, 67°, etc. have started appearing upon oxidation even at 200 °C. This shows that the oxidation of nano aluminium has started at 200 °C and is completed at 1000 °C.

A similar study was carried out with commercially available aluminium with mean particle size of 20 μm so as to compare the oxidation behaviour of coarse grain particles with those of nano-size particles. In order to estimate the percent fraction of γ-alumina in the corresponding samples of nano and coarse grain particles, the intensity associated with the most intense line for γ-alumina ($hkl = 440$) and that with c-Al ($hkl = 110$) has been

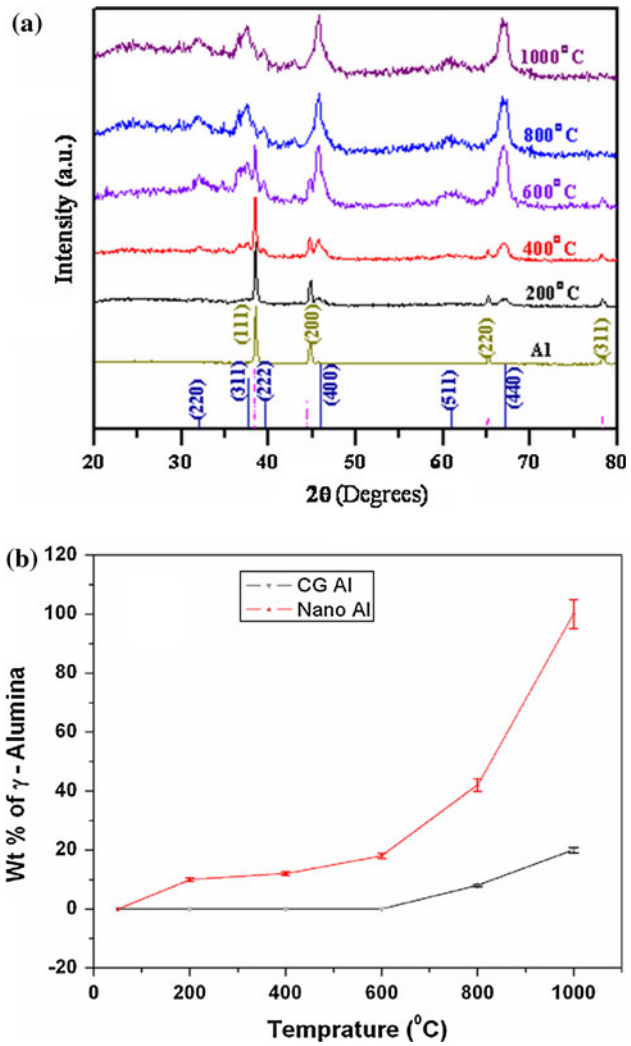

Fig. 1 **a** XRD patterns of as-synthesized nano aluminium and its oxides formed at 200, 400, 600, 800 and 1000 °C. Solid and dashed lines show the standard XRD line intensity patterns of γ-alumina and crystalline aluminium. **b** Comparison between the oxidation behaviours of nano Al and coarse grain aluminium as a function temperature of oxidation in air

considered. The percentage oxidation was estimated from the relation [25–27]

$$\text{wt\% of } \gamma\text{–Alumina} = {}^{100}/_{1 + 1.33(I_A/I_B)}$$

where,

I_B Intensity of (440) line of γ-Al_2O_3
I_A Intensity of (110) line of c-Al

Weight percentage of γ-alumina is plotted as a function of oxidation temperatures as shown in Fig. 1b. The curve indicates that the rate of oxidation of coarse-grain aluminium (mean size of 20 μm) is negligible up to 800 °C, and has increased by 19% at 1000 °C. In contrast nano aluminium exhibits much higher amount of oxidation at

each oxidation temperature, reaching a value of 100% at 1000 °C. This suggests that the enhanced surface area per unit volume of the nanoparticles plays a major role in the higher reactivity of these nanoparticles. Particles with average size of 60 nm diameter will have the surface to volume ratio of 10^8 whereas the coarse particles with average size of 20 μm diameter exhibit a value of 3×10^5. Thus the nanoparticles in this case exhibit an enhanced surface to volume ratio by three orders of magnitude as compared to the coarse particles.

Morphological analysis of the sample by TEM

It is interesting to see the morphological changes occurring in nanoparticles of aluminium after heating in an oxygen atmosphere at different temperatures ranging from 200 to 1000 °C. Figure 2a shows the TEM micrographs of the as-synthesized particles of aluminium. Here the particles are seen to be spherical in shape, varying in size from 30 to 80 nm. Each particle has an elongated feature. The information about crystalline structure was obtained from the Selected Area Electron Diffraction (SAED) pattern shown in Fig. 2b. The dot pattern indicates the crystalline nature of nanoparticles of aluminium.

Figure 2c shows the TEM micrograph of the nano aluminium heated in oxygen at 800 °C, whereas the corresponding diffraction pattern is presented in Fig. 2d. The spherical particles (30–100 nm in size) appear to be surrounded by a ring-like structure in which, the elongated wires attached to the particles have remained intact. From an analysis of the SAED pattern of these particles it is seen that the heat-treated particles are composed of γ-Al_2O_3 as well as crystalline aluminium.

Subsequent changes in the morphology of nano aluminium, when heated in oxygen at 1000 °C, are shown in Fig. 2e. Here part e of the figure shows the TEM micrograph demonstrating highly distorted and irregular shaped shell like features, varying in size from 80 to 120 nm. Part f shows the SAED pattern of the particles, confirming the presence of γ-Al_2O_3 alone.

In order to obtain finer details, HRTEM image was recorded for a single particle of the as-synthesized nano aluminium and those heated at 800 and 1000 °C. Figure 3a shows the HRTEM image corresponding to one of the sections of a single particle of as-synthesized Al. Figure 3b shows the HRTEM image of a 50 nm particle annealed at 800 °C. It is interesting to observe that the regions marked with (i) and (ii) posses closely matched lattice spacing corresponding to (111) planes of Al, whereas in region (iii) and (iv) we observe the lattice planes resembling with those corresponding to (111) plane of gamma Al_2O_3. The lattice imaging infers that the tail-like feature attached to the particle has single crystalline nature with lattice spacing of 0.46 nm corresponding to $d_{(111)}$ of gamma alumina.

Figure 4 shows the HRTEM image of a single particle heated in air at 1000 °C. The diameter of the particle is around 80 nm. Three different regions of this hollow particle are further magnified and projected in Fig. 4i, ii and iii. The inter-planar spacing in these three parts corresponds to $d_{(440)} = 1.4$ Å in region (i), $d_{(400)} = 1.9$ Å in region (ii), $d_{(400)} = 1.9$ Å in region (iii), of γ-Al_2O_3 [24]. It is thus clearly seen that after heating at 1000 °C the solid nanoparticle of Al have turned into hollow shell like structure of γ-Al_2O_3, slightly larger in size than the precursors and are distorted in shapes.

To understand the stoichiometric changes in the single nanoparticles we have used the Energy Dispersive X-Ray Analysis (EDX) by scanning over a single particle in TEM. Figure 5a, b show the TEM images of single particles, annealed at 800 and 1000 °C, and their corresponding EDX line-mappings. Both aluminium and oxygen are seen over the entire particle. The central regions of the particles have, however, lower concentrations because of the geometrical features of a hollow particle seen by the spectrometer. To differentiate the core region from the shell part, the spectral areas have been marked with I and II.

Thermogravimetric analysis

More precise information about the oxidation behaviour, responsible for the growth of hollow particles of aluminium oxide, was obtained by using the Thermogravimetric Analysis (TGA) technique. The results of this analysis are presented in Fig. 6 for coarse grain and nano aluminium particles. It is interesting to note that the particles of nano Al exhibit two-step oxidation processes, reaching a total weight gain of 50% at 1000 °C. This weight gain is indicative of complete oxidation (100% oxidation) of Al into Al_2O_3. The coarse-grain Al, on the other hand, shows incomplete oxidation even at 1000 °C attaining a weight gain of only 10%.

The two-step oxidation of nano aluminium has also been reported earlier [28]. The first step of the oxidation process appears at around 550 °C, before the melting point of aluminium (660 °C). This is supported by the fact that the smaller particles are more reactive and therefore the surface layer of the nanoparticles reacts at a much lower temperature [25] compared to that of coarse-grain Al. Such 'less reactive' behaviour of coarser particles (compared to the nanoparticles), has been well documented [29]. Pivkina et al. [30] have shown that the activation energy for combustion of aluminium nanoparticles is smaller than that of bulk aluminium. Park et al. [29] have employed quantitative, single particle mass spectroscopy to determine the size resolved kinetic rate constant for aluminium oxidation

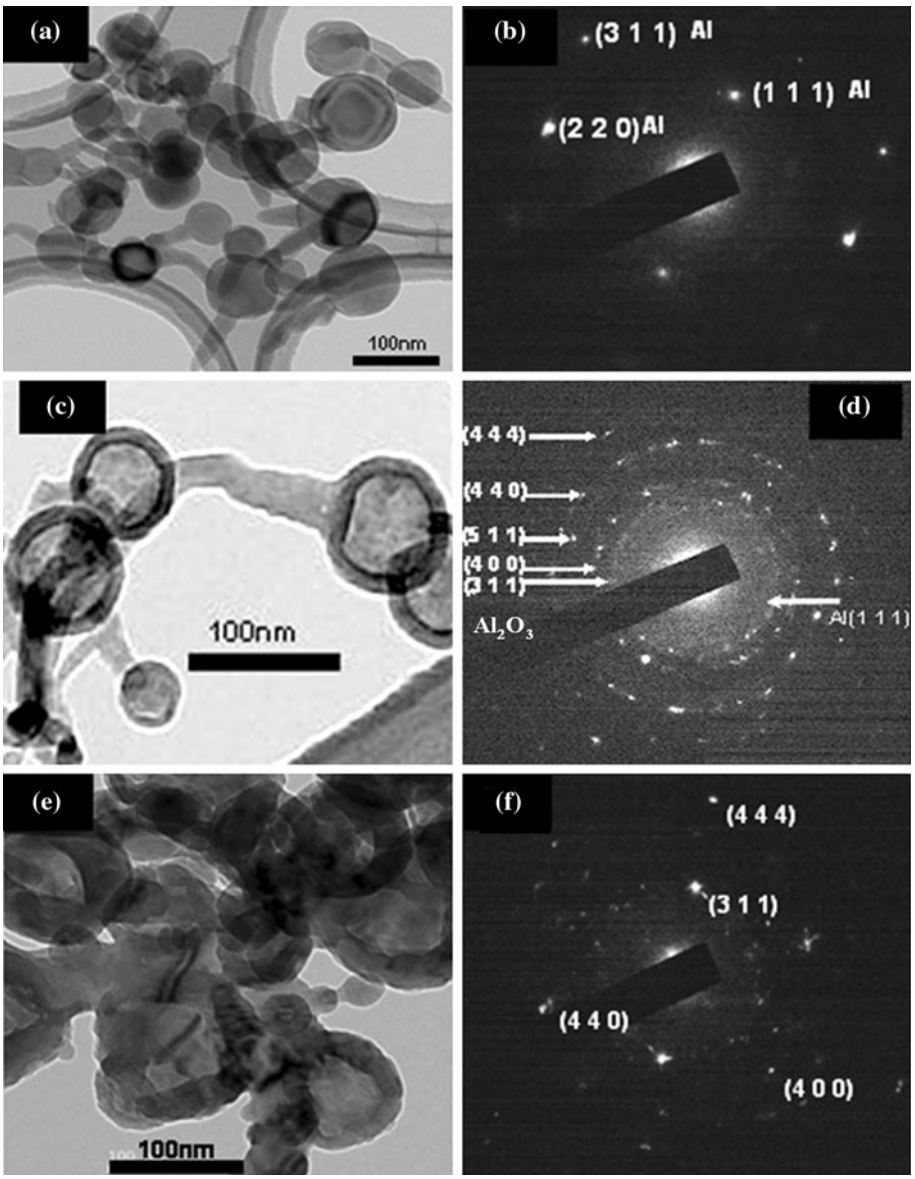

Fig. 2 Transmission electron micrographs for **a** as-synthesized nano Al, **c** heat treated at 800 °C, **e** heat treated at 1000 °C. Corresponding SAED patterns are in (**b**), (**d**) and (**f**)

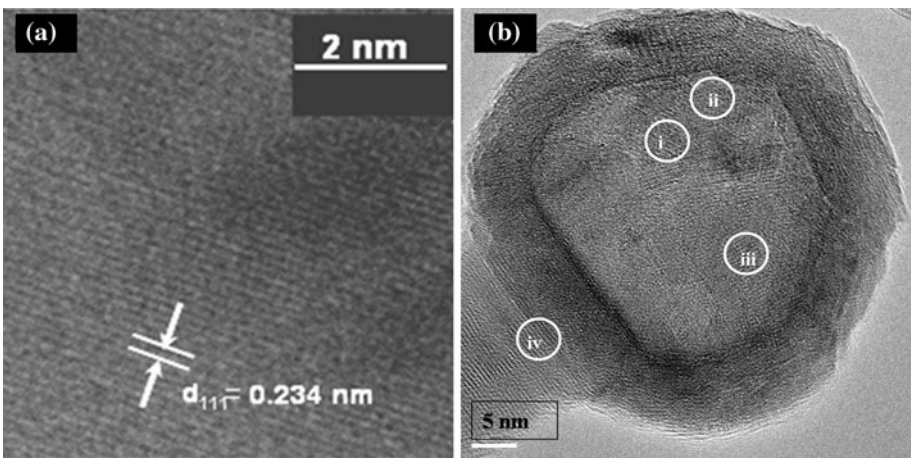

Fig. 3 HRTEM micrographs of **a** nano particle of as-synthesized aluminium **b** a single particle of Al heated in air up to 800 °C. Regions (*i*) and (*ii*) contain lattice planes corresponding to $d_{(111)} = 0.23$ nm for Al and the region (*iii*) and (*iv*) contain lattice planes with $d_{(111)} = 0.46$ nm for gamma alumina

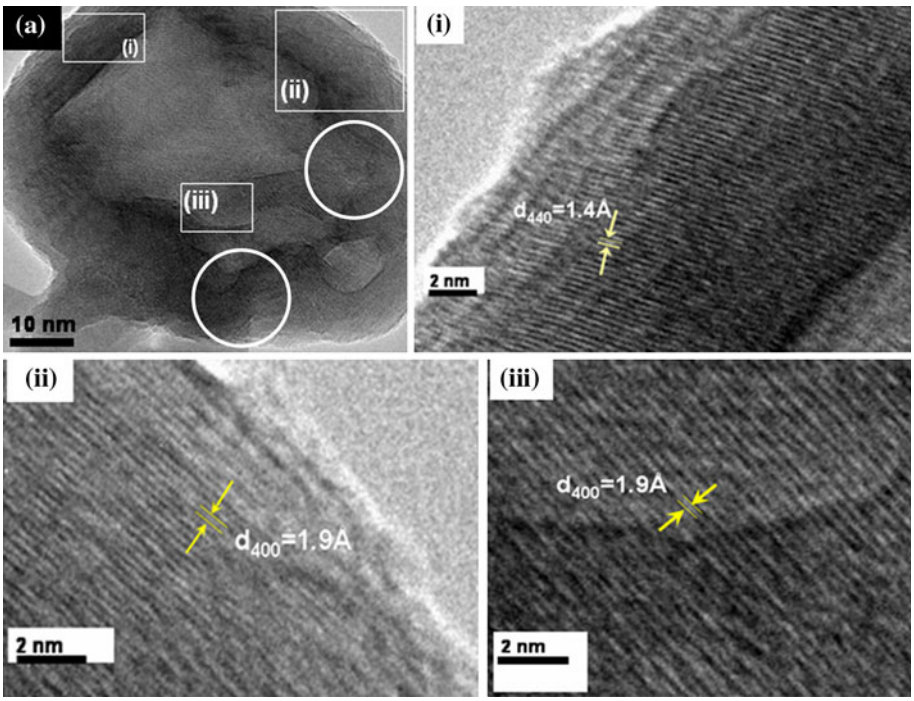

Fig. 4 **a** TEM image of single nanoparticle of γ-alumina formed after oxidizing the nanoparticle of Al at 1000 °C. **b**, **c** and **d** illustrate the HRTEM images of three different regions of nanoparticle as labelled by (*i*), (*ii*) and (*iii*), respectively in (**a**).The lattice spacings have been marked for (440) and (400) planes of gamma Al_2O_3. The *encircled areas* indicate the cracks which are closed after annealing

confirming that smaller particles are more reactive and that the oxidation is preceded by the phase transformation of aluminium. Here the growth of the oxide layer can be assumed due to the inward diffusion of oxygen and the outward diffusion of Al across the surface of the particles. In the first step of oxidation between 500 and 600 °C there is a weight gain of around 18%, and during this process the nanoparticle seems to get covered by a thin layer of oxide. According to experimental evidence [31] a thinner oxide film ($\sim$1 nm) is formed in small particles of Al rather than in its bulk state. Ijima [32, 33], by the dark field observation of the electron microscopy, found that the oxide film thickness of small particle of Si is recorded as the size becomes smaller. Detailed investigations on the size dependent oxide film have also been carried out with Al, Mg, Zn, Sn and Be by Sako et al. [34]. Moreover, it has also been proposed by Mott-Cabera [35] mechanism in the thin oxide films the adsorbed oxygen on the oxide surface is ionized by the electron which passes rapidly through the oxide layer. This is possible because of the quantum mechanical tunnel effect, or by the thermionic emission of electrons from the metal into the conduction band of the oxide layer, thus producing a strong electric field in the oxide. This causes the metal ions to dissolve into the interstitial sites of the oxide, resulting in their diffusion towards the surface. The oxide film, therefore, grows on the surface of the metal. At first the oxide grows, obeying the parabolic law, but at a later stage it reaches a constant thickness and the growth stops. This is validated by the relatively flat part of our TG curve between 600 and 800 °C for nano Al in Fig. 6, and is associated with a small weight gain of around 7%.

During the second step of oxidation from 800 to 1000 °C, we observe a major weight gain of around 25%, reaching a total value of 50% at 1000 °C. The second step in the TG curve for nano Al may arise because of the melting of the inner aluminium core of the particles, due to which the negative pressure increases at the Al–O and Al interface, and positive pressure increases at the outer surface of the oxide layer. A recent molecular dynamical calculation [36] confirms the presence of a large pressure inside the aluminium core and negative pressure (tension) of the oxide shell at these elevated temperatures. These results confirm that the oxide shell is unstable upon the melting of the aluminium core. They also show that the pressure rise in smaller particles is higher than that in larger particles, implying that smaller particles have a greater tendency to rupture. Moreover, due to its higher curvature, the oxide coating on smaller particles is under higher tension, and hence should rupture with greater ease as compared to the coatings on large particles. This causes breaking, cracking and puncture of the oxide surface of the spherical particle. The cracking of oxide layer and the resulting flow of Al melt from the core of the particles was also demonstrated in hot-stage TEM by Park et al. [30] and Rai et al. [37]. They observed the restructuring of the nanoparticles after rupture of the oxide layer when nano-Al particles were heated at 900 °C. As a result the melt reacts

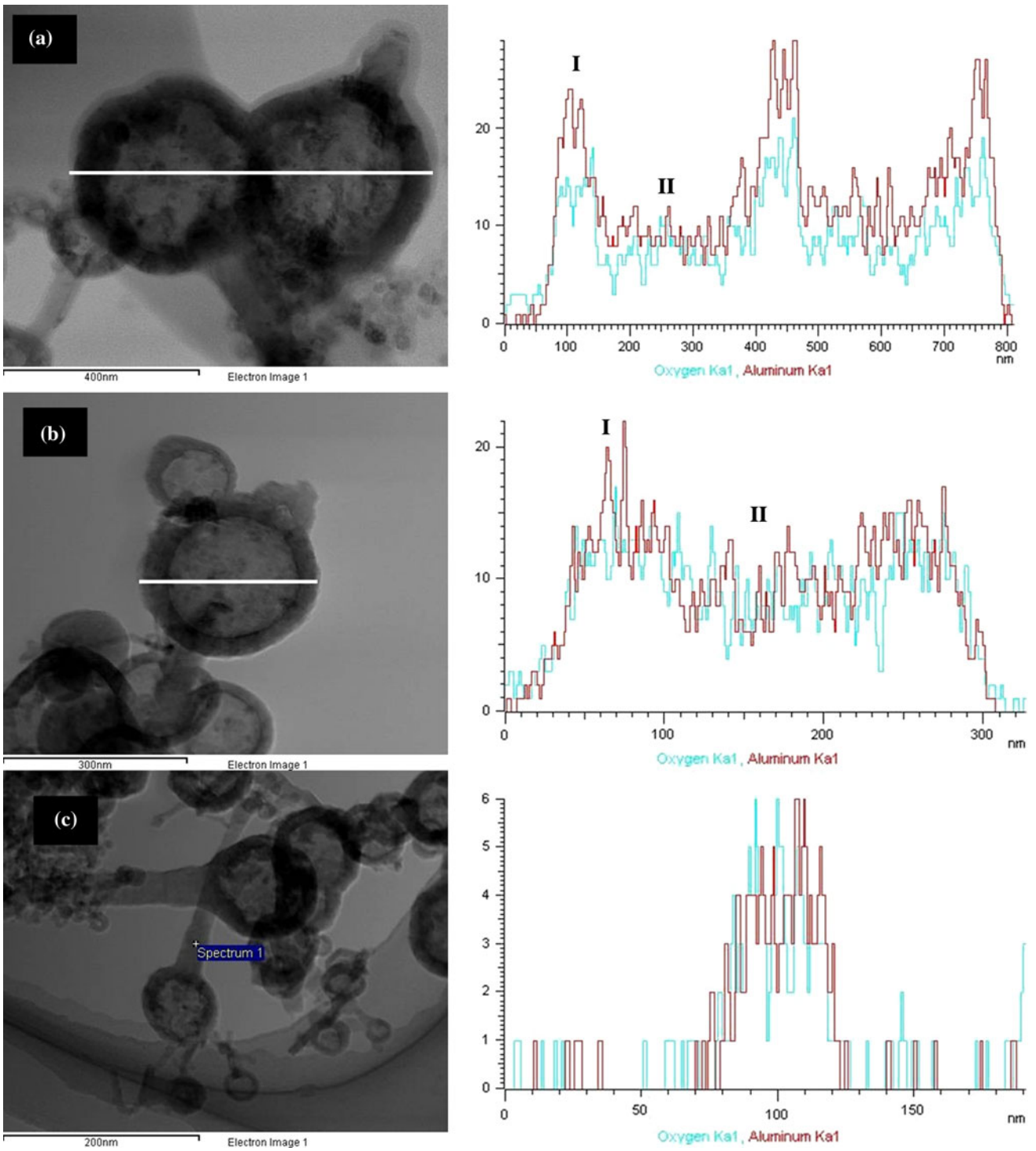

Fig. 5 **a** TEM image of couple of nanoparticles heat treated in air up to 800 °C and the corresponding EDX line mapping over the particles along the *marked line*. **b** TEM image of a single nanoparticle, heat treated in air up to 1000 °C and the corresponding EDX line mapping along the *marked line*. **c** EDX line mapping over a tail region which has been marked by (+) sign

completely with the oxygen aluminium moves outwards and oxygen inwards. However, as oxygen comes in contact with the aluminium melt; it again forms a solid oxide layer and closes the cracks. In this process the particle size would grow into a hollow sphere with having an irregular, distorted shape. Such distorted shapes are observed in our

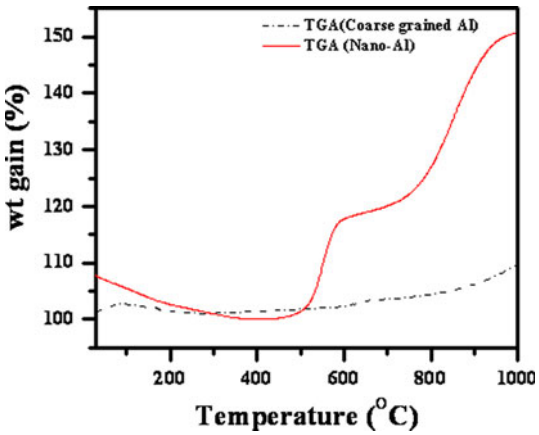

Fig. 6 Thermogravimetric analysis of nano-aluminium (*solid line*) and coarse grain aluminium (*dashed line*)

TEM micrographs shown in Fig. 2e for the nanoparticles heated to 1000 °C. Also there are some channels observed inside the wall of the hollow particle shown by the encircled part in the HRTEM image in Fig. 4a. This must have appeared on account of closing of the cracks.

The strength of the oxide layer also depends on its thickness; so the oxide layer present on big particles must be stronger than the oxide layer present on smaller particles. Once formed, an oxide layer on the larger particles is stable and does not allow further oxidation. The coarse particles of Al, therefore, do not get fully oxidized even at 1000 °C as shown by the TG curve corresponding to coarse grain in Fig. 6.

This speculation is confirmed by the TEM images of particles oxidized at 1000 °C shown in Fig. 2e. The image of the hollow particles oxidized at 800 °C is presented in Fig. 2c for comparison. The average diameter of the oxidized nano aluminium, with distorted shape, is seen to be around 120–130 nm, but 80–100 nm for virgin nano Al (Fig. 2a). The increase in size is expected due to the deposition of Al_2O_3 on the surface of the particle when the spherical nanoparticles rupture and the melt of aluminium flows.

The presence of un-reacted aluminium is also seen from the HRTEM images wherein the core of the nanoparticles heated at 800 °C exhibits Al at some parts along with its oxide. Such a presence was not observed in the HRTEM images of particle heated at 1000 °C. To confirm this finding the EDX mapping over the single particle presented in Fig. 5 can be used. The ratio of intensity of Al in shell (region I) to that in the core (region II) was estimated and was found to be 2.2–2.3 for the particle heated at 800 °C. This ratio increased to 3.3–3.4 for the particles heated at 1000 °C. This amounts to roughly 12% increased concentration of Al at the centre in the 800 °C annealed particles as compared to those annealed at 1000 °C.

Specific surface area measurement

Another important physical property of nano aluminium oxide is its specific surface area which should be larger for a hallow nanoparticle. A significant increase in the specific surface area, from 30 to 76 m^2/g, was measured for the solid [23] and hollow γ-alumina with nano-metric dimensions. This shows the effective potential of the catalysis of hollow nano-particles.

Conclusions

The article presents a simple method of growing hollow nanoparticles of γ-Al_2O_3, with a larger specific surface area. The thermal analysis shows that post-oxidation of nanoparticles of aluminium results in the rupture of particles on account of the increased pressure of the melt above 800 °C. In this process the cracks on the surface get closed by the growth of the oxide layer, thus forming the hollow structures. This is evidenced by the distorted shapes of the particles. The crystalline phase of the product particles has been confirmed to be γ-Al_2O_3 from XRD analysis. This article clearly brings out the differences between the oxidation features of coarse grain and nanoparticles of aluminium. The importance of nanoparticles as a precursor for the formation of γ-Al_2O_3 has been highlighted from this detailed analysis.

Acknowledgements The authors extend their thanks to ARMREB (India) for funding the project. S V. Bhoraskar acknowledges CSIR (India) for granting her the ES Scheme.

References

1. Ichinose N, Ozaki Y, Kashu S, James M (1992) Superfine particle technology. Springer, London
2. Andrievski RA (1994) J Mater Sci 29:614. doi:10.1007/BF00445970
3. Gleiter H (1989) Prog Mater Sci 33:223
4. Krell A, Blank P (1995) J Am Cerm Soc 78:1118
5. Huinan L, Webster TS (2007) Proceeding of bioengineering conference, IEEE 33rd Annual Northeast
6. Vassen R (1999) CFI Ceram Forum Int 76:19
7. Ratnasamy P, Sivsankar S (1980) Catal Rev Sci Eng 22:401
8. Furmsky E (1980) Catal Rev Sci Eng 22:371
9. Ciapetta FG, Wallace DN (1972) Catal Rev Sci Eng 5:67
10. Levin I, Brandon D (1998) J Am Cerm Soc 81:1995
11. Hirayama T (1976) J Am Ceram Soc 70:C122
12. Gribb AA, Banfield JF (1997) Am Miner 82:717
13. Borsella E, Botti S, Giorgi R, Martelli S, Turtu S, Zappa G (1993) Appl Phys Lett 63:1345
14. Nakajima H, Nakamura R (2010) Mater Sci Forum 638–642:67
15. Nanoko M, Matsumaru K, Ishizaki K (2006) Azojomo 2:1
16. Eun TH, Kim SH, Jeong WJ, Jeon SJ, Kim SH, Yang SM (2009) Chem Mater 21:201
17. Lee CW, Lee JS (2006) J Cerm Soc Jpn 114:923

18. Li XL, Lou TJ, Sun XM, Li YD (2004) Inorg Chem 43:5442
19. Guo XF, Kim YS, Kim GJ (2009) J Phys Chem C 113:8313
20. Kou H, Wang J, Pan Y, Guo J (2005) J Am Cerm Soc 88:1615
21. Cao F, Li DX (2009) Biomed Mater 4:025009 6pp
22. Pravdic G, Gani MSJ (1996) J Mater Sci 31:3487. doi:10.1007/BF00360753
23. Kulkarni NV, Karmakar S, Banerjee I, Sahasrabudhe SN, Das AK, Bhoraskar SV (2009) Met ResBull 44:581
24. JCPDS data: c-Aluminium [4–787], γ-Al2O3 [10–425]
25. Whiston C. X-ray methods, India edition (2008) Wiley India, New Delhi
26. Toraya H, Yoshimura M, Somiya S (1984) J Am Ceram Soc 67: C119
27. Wu NL, Wu TF (2000) J Am Ceram Soc 83:3225
28. Il'in AP, Gromov AA, Yablunovskii GV (2001) Comb Expl Shock Waves 37:418
29. Park K, Lee D, Rai A, Mukherjee D, Zachariah MR (2005) J Phys Chem B 109:7290
30. Pivkina A, Streletskii A, Kolbanev I, Ul'yanova P, Frolov Yu, Butyagin P (2004) J Mater Sci 39:5451. doi:10.1023/B:JMSC.0000039264.33941.82
31. Ramaswamy AL, Kaste P (2005) J Energ Mater 23:1
32. Iijima SJ (1987) Appl Phys 26:357
33. Iijima SJ (1987) J Appl Phys 26:365
34. Sako S, Ohshima K, Fujita T (1990) J Phys Soc Jpn 59:662
35. Cabrera N, Mott NF (1948) Rep Prog Phys 12:163
36. Campbell T, Kalia RK, Nakano A, Vashishta P, Ogata S, Rodgers S (1999) Phys Rev Lett 82:4866
37. Rai A, Lee D, Park K, Zachariah MR (2004) J Phys Chem B 108:14793